Research Article

Investigation of microstructure, ferroelectric and dielectric behavior of $CaCu_3Ti_{(4-x)}Mn_xO_{12}$ perovskites synthesized through semi-wet route

Santosh Pandey[1] · **K. D. Mandal**[1]

Received: 26 August 2019 / Accepted: 7 November 2019 / Published online: 30 November 2019

Abstract
The Mn-doped CCTO ($CaCu_3Ti_{(4-x)}Mn_xO_{12}$ system $x = 0.25$, 0.50 and 1.00) ceramic has been synthesized by using metal nitrates and solid TiO_2 powder sintered at 1223 K for 8 h. The crystal phase of CCTMO was confirmed by the XRD at 1223 K for 8 h. The phase-structure, as well as microstructure, was examined by XRD and SEM, respectively. The SEM micrograph revealed the effect of Mn concentration on grain size and grain formation. The bright-field TEM image of the system confirmed the particle size in the range of 22–30 nm. The stoichiometry and purity of synthesized material were observed by EDX. The investigated dielectric permittivity and tangent loss were found to be 150 and 0.6, respectively, at room temperature (10 kHz), which may be used in electronic devices.

Keywords Semi-wet route · Ceramic · Microstructure · Dielectric properties

1 Introduction

An unusual and promising perovskite oxide $CaCu_3T_4O_{12}$ (CCTO) was recently found at extraordinarily high dielectric permittivity at room temperature in the range of 10^4–10^6, which is frequency independent and possesses good temperature stability over a broad temperature range from 100 to 800 K [1–3]. The temperature dependency and high dielectric constant of CCTO have attracted much of the attention of scientists. Such special physical behavior and being Ba/Pb free make it a promising application for microelectronics devices, such as an actual application of CCTO perovskites in the modern electronic devices; but the main problems of this type of ceramic material is its high tangent loss and large linkage current. The CCTO ceramic has been combined in a 1:3 ratio of A-site-ordered perovskite $A_1Cu_3Ti_4O_{12}$ with space group Im3, containing octahedral Ti-site of TiO_6 and was also combined with A-site of Cu square-planar [1, 4, 5]. The extrinsic origin relaxation resulting from contact effect, spatial inhomogeneity and the internal barrier layer capacitor mechanism (IBLC) is frequently accepted to be the cause of the colossal dielectric constant (CDC); and intrinsic relaxation for colossal dielectric constant is also active which is responsible for electrical behavior of $CaCu_3Ti_4O_{12}$ (CCTO), depending on their synthesis route [6–8]. Previous researches on CCTO recommended that the local dipoles induced by doping on Ti-site could be responsible for the high dielectric constant [9]. Scientists across the globe carried out an extensive study over the mechanism of dependable high dielectric constant (ε_r) of CCTO but have not reached a definitive conclusion. The internal boundary layer capacitor (IBLC) mechanism explained the high dielectric constant in CCTO ceramics [10–12]. According to IBLC theory, in CCTO ceramic, the dielectric variation is produced from the semiconducting grains and insulating grains boundary (GB). Therefore, the variation on microstructure can explain up to a good extent by studying the dielectric properties [13, 14]. Recently, researches revealed that the mixed metal-valent structure (e.g., Ti^{3+}/Ti^{4+}, Fe^{2+}/Fe^{3+}, Cu^{+}/Cu^{2+}, Mn^{3+}/Mn4+ and so on) interrelated ordinary behavior of CDC materials [15, 16], which might directly affect

✉ K. D. Mandal, kdmandal.apc@itbhu.ac.in | [1]Department of Chemistry, Indian Institute of Technology (BHU), Varanasi, UP 221005, India.

the dielectrical behavior of CCTO ceramics. In this way, the different compositions of Mn-doping in CCTO change the grain boundary and also produce a large effect on dielectric behaviors [14]. The microstructure of CCTO ceramic also changes considerably with a small variation in sintering temperature due to irregular grain growth behavior of Mn-doped ceramics [16, 18]. The metal ion doping in CCTO was found to be a good method that strongly controls microstructure, particle size, electrical properties of grains (semiconducting/insulating behaviors) and grain boundaries (dielectric constant, thickness and resistance) [19]. On the basis of structural investigation, the part TiO_6 octahedra are sufficient to produce local distortions, which is effectively responsible for the pure ferroelectric properties of CCTO ceramic. In fact, the ferroelectric behavior was observed in CCTO in a broad temperature range. Furthermore, in comparison with other isostructural compounds, only the CCTO has possessed high dielectric constant [20, 21].

CCTO was synthesized by solid-state method from the metal oxide at high temperature. This method needed a long reaction time, high calcination and sintering temperature. In addition, some other secondary phases (CuO, TiO_2 and Cu_2TiO_3) may also come out during synthesis [22, 23]. On the other hand, synthesis by a chemical solution process such as sol–gel using metal alkoxide gives intimate and uniform mixing of the metal ion at the atomic scale. In this route, titanium isopropoxide $Ti(OR)_4$ is very costly. So, we have synthesized $CaCu_3Ti_{(4-x)}Mn_xO_{12}$ by a semi-wet route and reported their comparative studies of synthesis, microstructure, dielectric and ferroelectric properties. In this method, metal nitrates have been used in powder form instead of using costly titanium isopropoxide.

The CCTMO was calcined as well as sintered at 973 K and 1223 K, respectively, for 8 h. The results confirmed that the Mn-doping can make the dielectric constant decrease with increasing Mn concentration about two orders of magnitude (from 10^4–10^2) [21, 24]. These procedures possess the advantage to refine permittivity, dielectric loss and the ferromagnetic response of Mn-doped CCTO ceramics.

2 Experimental details

2.1 Materials and synthesis

CCTMO was synthesized through a semi-wet route. In this method, chemicals calcium nitrate $Ca(NO_3)_2{\cdot}4H_2O$ (98% Merck, India), copper nitrate $Cu(NO_3)_2{\cdot}3H_2O$ (99% Merck, India), manganese acetate $Mn(CH_3COO)_2{\cdot}4H_2O$ (99% Merck, India) and titanium oxide TiO_2 (99% Merck, India), were taken in stoichiometric amounts in molar ratio. The solution of $Ca(NO_3)_2{\cdot}4H_2O$, $Cu(NO_3)_2{\cdot}3H_2O$, and $Mn(CH_3COO)_2{\cdot}4H_2O$ was prepared in distilled water. All the solutions were mixed together in a beaker, and a stoichiometric amount of solid TiO_2 was added in solution. The calculated amount of citric acid (99.5%, Merck India) equivalent to metal ions was dissolved in distilled water and mixed with the solution. The resulting solution was heated on a hot-plate magnetic stirrer at 348–353 K to evaporate water and allows for self-ignition. A fluffy mass of CCTMO powders was obtained after the removal of a lot of gases. Citric acid was used as a complexing agent that acts as fuel in the ignition step. The resulting CCTMO powder was ground with the help of agate and mortar to make a fine powder. The powder was calcined at 1073 K for 6 h. Calcined powder was used to make cylindrical pellets using 2% PVA as a binder on applying 3 tons of pressure using hydraulic pressure for 90 s. Finally, the CCTMO pellets were sintered at 1373 K for 8 h.

2.2 Characterization

The crystalline phase of CCTMO ceramic-sintered sample was identified by X-ray diffractometer (Rigaku miniflex 600, Japan) applying Cu-kα radiation with wavelength 1.5418 Å. The microstructure and elemental composition were confirmed by scanning electron microscope (ZEISS; model EVO18 research, Germany) attached with an energy-dispersive X-ray (EDX) analyzer (Oxford instrument, USA). The particle size was examined by a high-resolution transmission electron microscope (HR-TEM, Technai G2 20 S-Twin). For HR-TEM characterization, the sample was dispersed in acetone and sonicated for 2 h. This suspension was deposited on a carbon-coated copper grid and dried in oven for 4 h. The thickness and surface morphology were analyzed using atomic force microscopy (NTEGRA Prima, Germany). The dielectric data of silver-coated cylindrical pellets were examined by LCR meter (PSM1735, NumetriQN$_4$L, UK). The ferroelectric behaviors of sintered CCTMO ceramics were measured by the ferroelectric tracer (automatic *P*–*E* loop tracer, Marin India).

3 Results and discussion

3.1 Microstructure studies

The X-ray diffraction pattern of $CaCu_3Ti_{4-x}Mn_xO_{12}$ ($x = 0.25$, 0.50 and 1.00) ceramics powder sintered at 1223 K for 8 h is shown in Fig. 1. It illustrates the presence of CCTO as a major phase along with the minor phase of TiO_2. The diffraction patterns are correctly matched with JCPDS (card no. 21-0140), which confirms the presence of the major phase formation of CCTO with the minor secondary phase

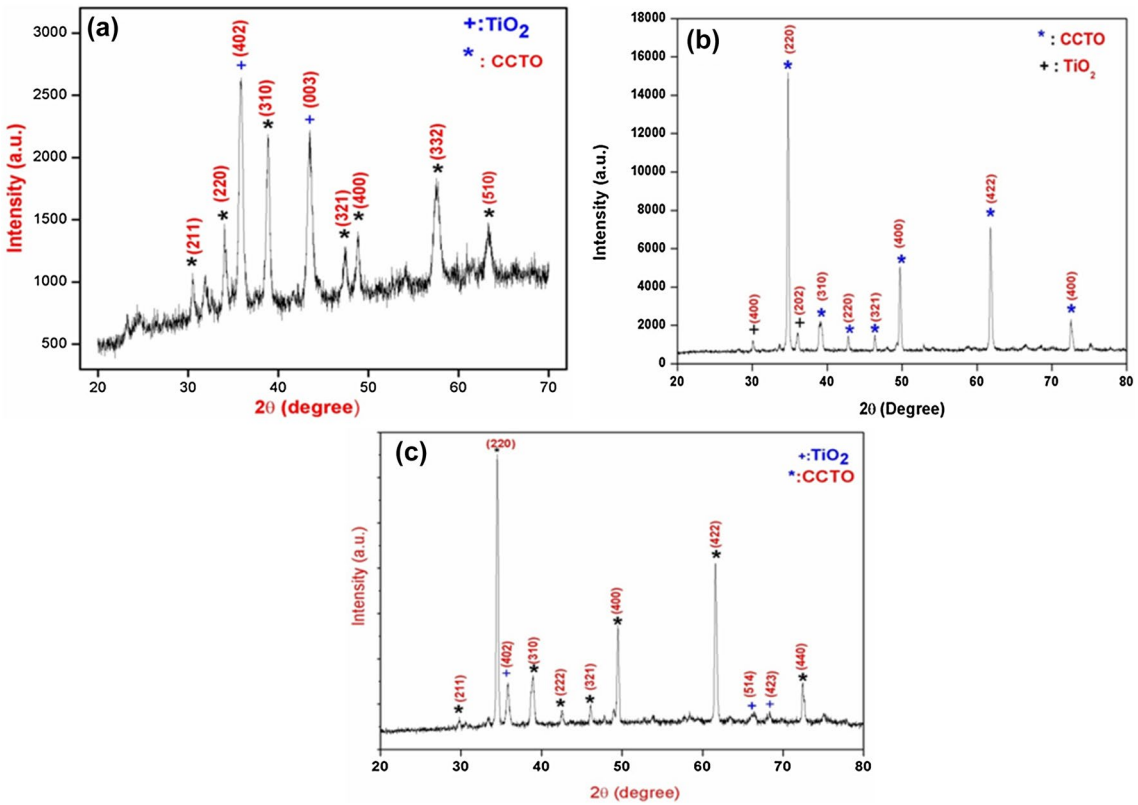

Fig. 1 XRD patterns of $CaCu_3Ti_{4-x}Mn_xO_{12}$ **a** $x=0.25$, **b** $x=0.50$, **c** $x=1.00$ sintered at 1223 K for 8 h

with JCPDS (card no. 46-1238) of TiO_2 [23]. The structure of the CCTO sample does not change after Mn-doping sintered at 1223 K for 8 h, and it remains cubical in all compositions of Mn-doped CCTO samples. The crystallite size (D) of CCTMO was calculated by using the Debye–Scherrer formula, which is represented as follows in eq. (1).

$$D = \frac{K\lambda}{\beta COS\theta} \tag{1}$$

where D is crystallite size, k is constant equal to 0.89, λ is a wavelength of X-ray, θ is the Bragg diffraction angle and β is the full width at half maximum (FWHM) in radians. For the calculation of the correct value of crystallite size, the line broadening due to instrumental effect was eliminated by using a standard sample (silicon wafer) for XRD data. The average crystalline size of CCTMO was calculated as 16 nm, 40 nm and 32 nm at different Mn-doping concentrations $x=0.25$, 0.50, and 1.00 ($CaCu_3Ti_{4-x}Mn_xO_{12}$), respectively. The lattice parameter increases with an increased doping concentration of Mn in CCTO due to increases in density.

Figure 2 illustrates the bright-field TEM images (a, b and c) along with the corresponding SEAD pattern (d, e and f) of $CaCu_3Ti_{4-x}Mn_xO_{12}$ ceramics with ($x=0.25$, 0.50 and 1.00) sintered at 1223 K for 8 h. The observed particle size measured by TEM was found to be 23 ± 10 nm, 31 ± 10 nm and 24 ± 10 nm at a different doping concentration of Mn ($x=0.25$, 0.50 and 1.00) in $CaCu_3Ti_{4-x}Mn_xO_{12}$ ceramic. The particle size calculated by TEM is close to crystallite size observed by X-ray diffraction. Figure 2(d, e and f) shows the selected area diffraction (SAED) pattern, which confirms that the free-standing crystal shows the single crystal in nature [25].

Figure 3a–c presents the SEM micrograph of $CaCu_3Ti_{4-x}Mn_xO$ ($x=0.25$, 0.50 and 1.00) ceramics sample sintered at 1223 K for 8 h. The doping of Mn in CCTO greatly affects the microstructures [11]. The microstructural progress showed a relatively different behavior according to the doped Mn content. The average grain size of CCTMO ceramic at low doped Mn content ($x=0.25$) has been observed at 1.90 µm. The average grain size of CCTMO at high Mn-doped ($x=0.50$ and 1.00) content has been observed as 1.57 µm and 1.78 µm, respectively. The grain size uniformly increases with increasing Mn compositions. The increase in grain size with increasing Mn concentration may be due to enlarged grain boundary mobility [12]. Figure 3d–f presents the EDX spectra of CCTMO ceramic sintered at 1223 K for 8 h, which confirms the presence of Ca, Cu, Mn, Ti and O elements. The atomic

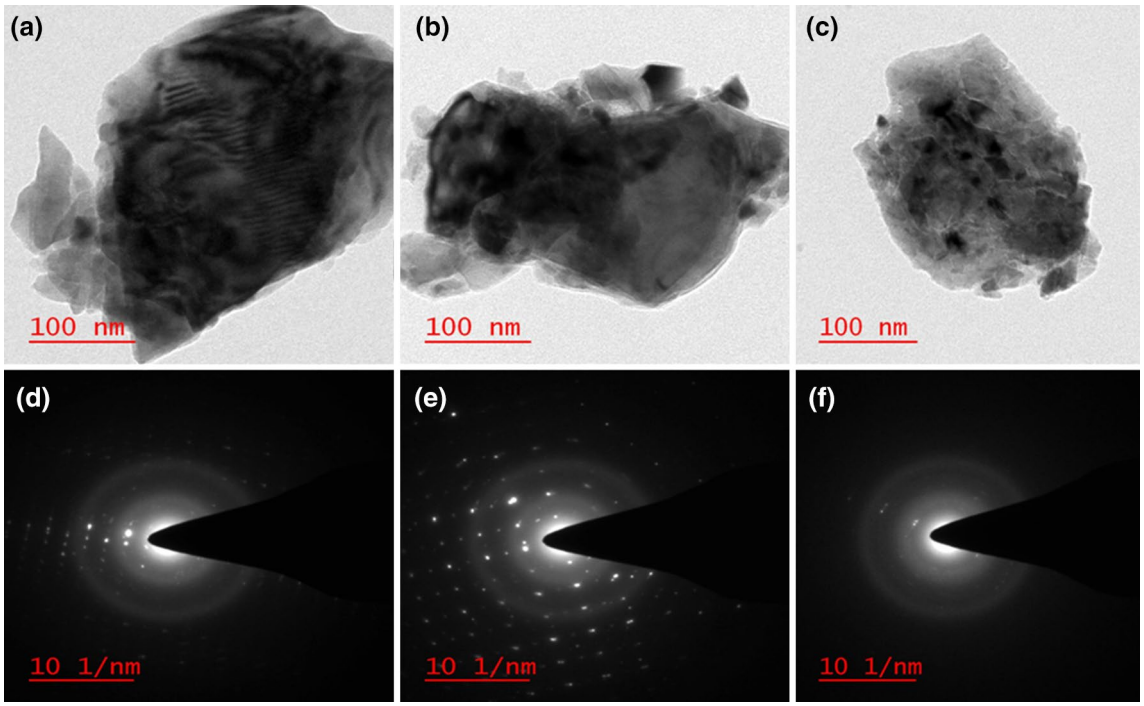

Fig. 2 Bright-field TEM images and their corresponding SAED patterns of sintered $CaCu_3Ti_{4-x}Mn_xO_{12}$ ceramic (0.25, 0.50 and 1.00)

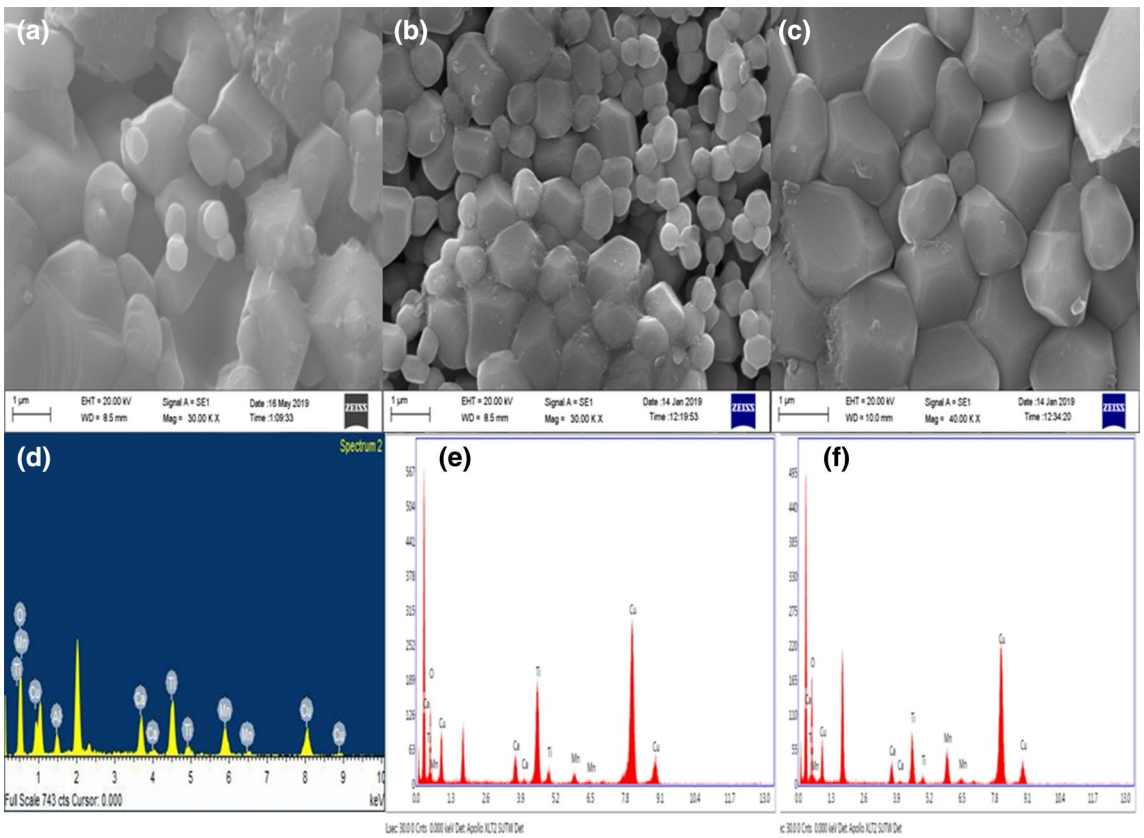

Fig. 3 SEM micrograph of $CaCu_3Ti_{4-x}Mn_xO_{12}$ ceramics **a** $x=0.25$, **b** $x=0.50$, **c** $x=1.00$ and EDX spectra of $CaCu_3Ti_{4-x}Mn_xO_{12}$ ceramics **d** $x=0.25$, **e** $x=0.50$, **f** $x=1.00$ sintered at 1223 K for 8 h

percentage of Ca, Cu, Mn, Ti, and O elements is shown in Table 1 with different compositions confirming the stoichiometry and purity of CCTMO ceramic materials.

Figure 4a depicts 2D atomic force micrograph (AFM) of $CaCu_3Ti_{4-x}Mn_xO_{12}$ ($x=1.00$) ceramic sintered at 1223 K for 8 h. The 2D micrograph illustrates the bimodal structures of grains separated from the grain boundary [26]. The average roughness (R_a) and root mean square roughness (R_q) were found to be 72 nm and 90 nm, respectively, on a scanned area 20 µm × 20 µm. The maximum peak valley depth (R_v) of a 2D structure is found to be 241 µm. Figure 4b shows the distribution of the particles observed in the 3D structure. Figure 4c presents the histogram of grain size, in which the majority of grains are obtained in the range of 1.0–1.4 µm. The average grain size estimated by a 2D micrograph was found to be 1.2 µm out of 191 gains, as shown in Fig. 4c, which is supported by SEM investigation.

Table 1 Atomic percentage of elements for $CaCu_3Ti_{(4-x)}Mn_xO_{12}$ ceramics ($x=0.25$, 0.50 and 1.00) sintered at 1223 K for 8 h

Composition	Atomic percent of elements				
	Ca (%)	Cu (%)	Ti (%)	Mn (%)	O (%)
0.25	5.00	15.00	18.75	1.25	60.00
0.50	5.00	15.00	17.50	2.50	60.00
1.00	5.00	15.00	15.00	5.00	60.00

3.2 Dielectric studies

The frequency-dependent dielectric constant (ε_r) at room temperature is shown in Fig. 5. The dielectric permittivity (ε_r) decreases with increasing frequency. The value of dielectric constant (ε_r) at room temperature at 10 kHz was found to be 148, 122 and 105 for $CaCu_3Ti_{4-x}Mn_xO_{12}$ ($x=0.25$, 0.50 and 1.00) ceramic samples sintered at 1223 K for 8 h. Figure 6 shows the tangent loss (tan δ) against frequency at room temperature (10 kHz). The tangent loss (tan δ) of $CaCu_3Ti_{4-x}Mn_xO_{12}$ ($x=0.25$, 0.50 and 1.00) ceramic was found to be 0.4, 0.3 and 0.6 at 10 kHz. The tangent loss in Mn-doped CCTO was found to be 0.5 at 10 kHz for all measured compositions [27, 28]. These effects create semiconducting grains and insulating boundaries as published in many ceramic oxides by using the IBLC mechanism in different CCTMO compositions [29]. The tangent

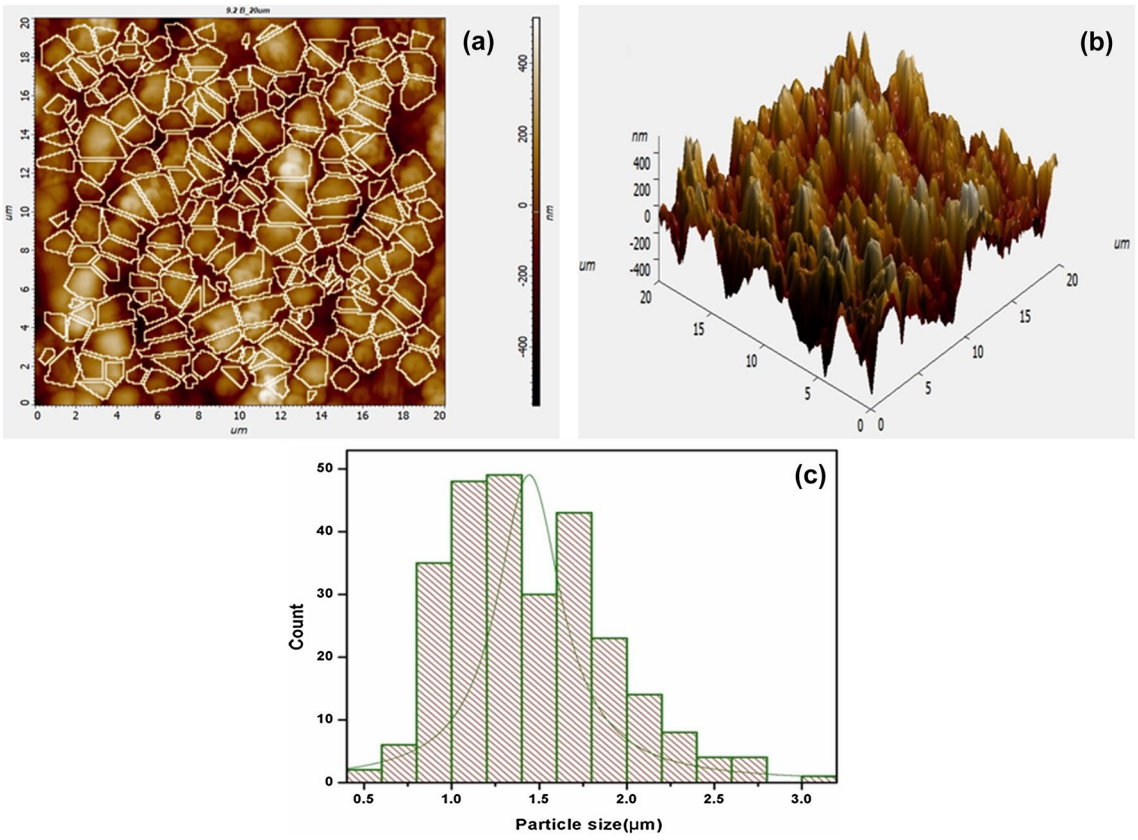

Fig. 4 AFM images of $CaCu_3Ti_{4-x}Mn_xO_{12}$ ($x=1.00$) ceramics sintered at 1223 K for 8 h **a** 2-dimensional structure, **b** 3-dimensional structure, **c** bar diagram of particle size

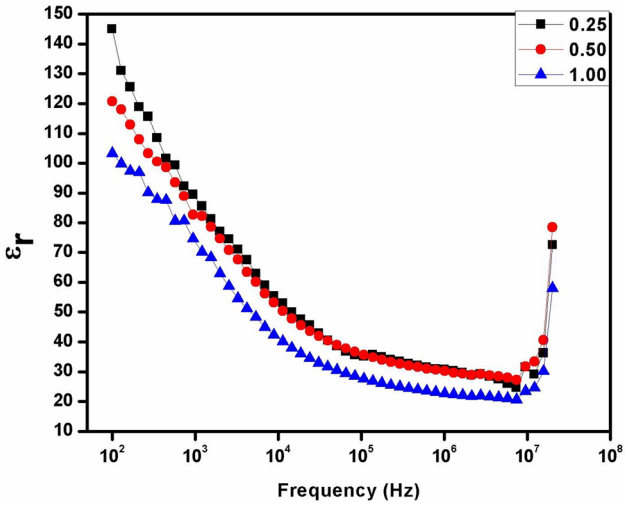

Fig. 5 Dielectric constant (ε_r) as the function of frequency for $CaCu_3Ti_{4-x}Mn_xO_{12}$ ceramics ($x = 0.25$, 0.50 and 1.00) sintered at 1223 K for 8 h

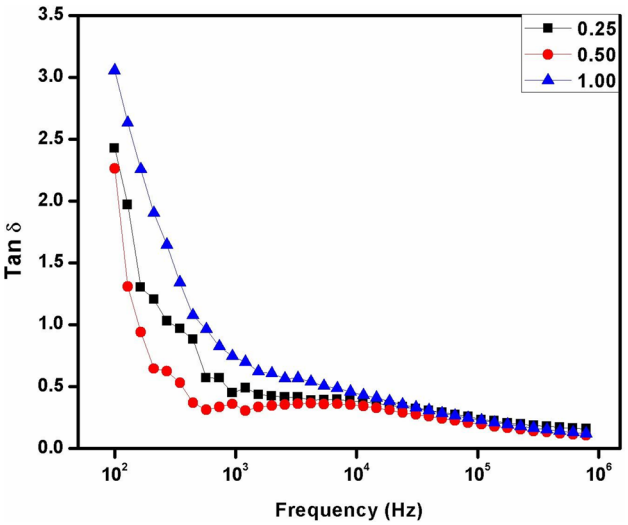

Fig. 6 Dielectric loss (tan δ) as the function frequency $CaCu_3Ti_{4-x}Mn_xO_{12}$ ceramics ($x = 0.25$, 50 and 1.00) sintered at 1223 K for 8 h

loss curves observed in the Mn-doped CCTO are due to thermally activated relaxation [30].

Figure 7 depicts that the polarization against the electric field *P–E* hysteresis loop of different compositions of Mn-doped CCTO ceramic was detected at room temperature (313 K). This calculation was carried out at a frequency of 150 Hz. With the increasing temperature, the nature of the loop has been changed which becomes slimmer. This property of the *P–E* loop shows the evolution process to relaxor ferroelectrics [31]. At the given electric field, resultant remnant polarization

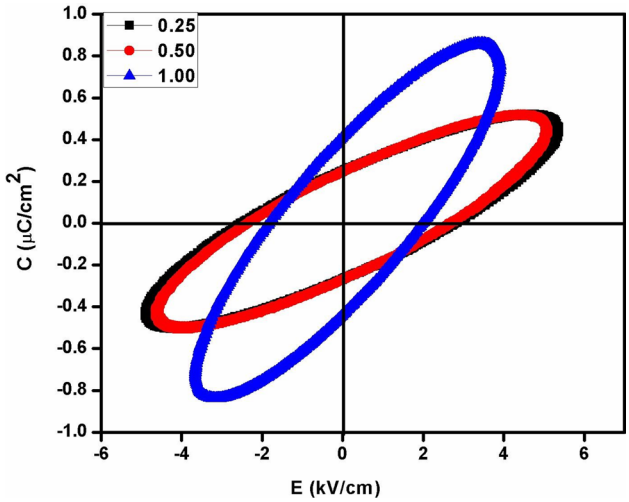

Fig. 7 *P–E* hysteresis loop for $CaCu_3Ti_{4-x}Mn_xO_{12}$ ceramics ($x = 0.25$, 0.50 and 1.00) at room temperature

(P_r) increases with increasing Mn concentration in CCTO samples. The measured value of remnant polarization (Pr) for $CaCu_3T_{(4-x)}Mn_xO_{12}$ ceramic with compositions $x = 0.25$, 0.50 and 1.00 is 0.259, 0.258 and 0.427 μC/cm^2 at 1223 K for 8 h. On the applying, high electric field saturation was not found in the *P–E* hystersis loop for $CaCu_3Ti_{(4-x)}Mn_xO_{12}$ ceramicx ($x = 0.25$, 0.50 and 1.00) at room temperature. The absence of saturation polarization is due to the resistor joint in parallel, indicating the lossy capacitor nature of the materials [32].

4 Conclusions

$CaCu_3T_{(4-x)}Mn_xO_{12}$ ($x = 0.25$, 0.50 and 1.00) was successfully synthesized by semi-wet route. Solid TiO_2 powder and metal nitrates are used in the preparation of CCTMO. The major phase as CCTO along with the minor phase of TiO_2 was confirmed by XRD sintered at 1223 K for 8 h. The SEM micrograph shows the clear grain and grain boundaries with an average grain size in the range of 1–2 μm. The particle size was measured by the TEM technique. The dielectric constant decreases with increasing Mn concentration in CCTMO ceramic. The measured tangent loss decreases with increasing frequency. The stoichiometry and purity of CCTMO ceramic were confirmed by the EDX analysis.

Acknowledgements The author would like to thank the in-charge of the central instrument facility centre (CIFC), IIT (BHU), Varanasi, for SEM, TEM and AFM facilities. One of the authors Santosh Pandey is grateful to IIT (BHU) for financial support for teaching assistantship.

Compliance with ethical standards

Conflict of interest There is no conflict of interest among the authors.

References

1. Thomas AK, Abraham K, Thomas J, Saban KV (2017) Electrical and dielectric behaviour of $Na_{0.5}La_{0.25}Sm_{0·25}Cu_3Ti_4O_{12}$ ceramics investigated by impedance and modulus spectroscopy. J Asian Ceram 5:56–61
2. Gavrilyachenko VG, Kabirov YV, Panchenko EM, Sitalo EI, Gavrilyachenko TV, Milov EV, Lyanguzov NV (2013) Specific features of the dielectric spectrum of $CaCu_3Ti_4O_{12}$ in the low-frequency range. Phys Solid State 55:1651–1654
3. Jesurani S, Kanagesan S, Velmurugan R, Thirupathi C, Sivakumar M, Kalaivani T (2011) Nanoparticles of the giant dielectric material, calcium copper titanate from a sol–gel technique. Mater Lett 65:3305–3308
4. Schmidt R, Stennett MC, Hyatt NC, PokornY J, Prado-Gonjal J, Li M, Sinclair DC (2012) Effects of sintering temperature on the internal barrier layer capacitor (IBLC) structure in $CaCu_3Ti_4O_{12}$ (CCTO) ceramics. J Eur Ceram Soc 32:3313–3323
5. Aliabadi TN, Alizadeh P (2019) Microstructure and dielectric properties of CCTO glass-ceramic prepared by the melt-quenching method. Ceram Int 45(15):19316–19322
6. Riquet G, Marinel S, Bréard Y, Harnois C (2019) Sintering mechanism and grain growth in $CaCu_3Ti_4O_{12}$ ceramics. Ceram Int 45:9185–9191
7. Kim BK, Lee HS, Lee JW, Lee SE, Cho YS (2010) Dielectric and grain-boundary characteristics of hot pressed $CaCu_3Ti_4O_{12}$. J Am Ceram Soc 93:2419–2422
8. Thongbai P, Putasaeng B, Yamwong T, Maensiri S (2012) Modified giant dielectric properties of samarium doped $CaCu_3Ti_4O_{12}$ ceramics. Mater Res Bull 47:2257–2263
9. Fan J, Leng S, Cao Z, He W, Gao Y, Liu J, Li G (2019) Colossal permittivity of Sb and Ga co-doped rutile TiO_2 ceramics. Ceram Int 45:1001–1010
10. Li M, Sinclair DC, West AR (2011) Extrinsic origins of the apparent relaxorlike behavior in $CaCu_3Ti_4O_{12}$ ceramics at high temperatures: a cautionary tale. J Appl Phys 109:084106
11. Singh L, Rai US, Mandal KD (2012) Influence of Zn-doping on microstructures and dielectric properties in $CaCu_3Ti_4O_{12}$ ceramic synthesised by semi-wet route. Adv Appl Ceram 111:374–380
12. Senda S, Rhouma S, Torkani E, Megriche A, Autret C (2017) Effect of nickel substitution on electrical and microstructural properties of $CaCu_3Ti_4O_{12}$ ceramic. J Alloys Compd 698:152–158
13. Kim KM, Lee JH, Lee KM, Kim DY, Riu DH, Lee SB (2008) Microstructural evolution and dielectric properties of Cu-deficient and Cu-excess $CaCu_3Ti_4O_{12}$ ceramics. Bull Mater Sci 43:284–291
14. Amaral F, Valente MA, Costa LC (2010) Dielectric properties of $CaCu_3Ti_4O_{12}$ (CCTO) doped with GeO2. J Non-Cryst Solids 356:822–827
15. Sun X, Wang C, Wang G, Lei C, Li T, Liu L (2013) Low-temperature dielectric relaxations associated with mixed-valent structure in $Na_{0.5}Bi_{0.5}Cu_3Ti_4O_{12}$. J Am Ceram Soc 96:1497–1503
16. Sun X, Wang C, Wang G, Lei C, Li T, Liu L (2013) Low-temperature relaxations associated with mixed-valent structure in Sr_2TiMnO_6. J Am Ceram Soc 96:513–518
17. Kim KM, Kim SJ, Lee JH, Kim DY (2007) Microstructural evolution and dielectric properties of SiO_2-doped $CaCu_3Ti_4O_{12}$ ceramics. J Eur Ceram Soc 27:3991–3995
18. Kawrani S, Boulos M, Cornu D, Bechelany M (2019) From synthesis to applications: copper calcium titanate (CCTO) and its magnetic and photocatalytic properties. Chem Open 8:922–950
19. Kashyap R, Thakur OP, Tandon RP (2012) Study of structural, dielectric and electrical conduction behaviour of Gd substituted $CaCu_3Ti_4O_{12}$ ceramics. Ceram Int 38:3029–3037
20. Kumari R, Ahlawat N, Agarwal A, Sanghi S, Sindhu M, Rani S (2018) Effect of doping of alkaline metal ions on structural and electrical properties of $Bi_{0·8}M_{0·2}FeO_3$-modified $Na_{0.5}Bi_{0.5}TiO_3$ ceramics (M = Ca, Sr, and Ba). J Alloys Compd 747:712–720
21. Li M, Chen XL, Zhang DF, Wang WY, Wang WJ (2010) Humidity sensitive properties of pure and Mg-doped $CaCu_3Ti_4O_{12}$. Sens Actuators B Chem 147:447–452
22. Lin YH, Deng W, Xu W, Liu Y, Chen D, Zhang X, Nan CW (2012) Abnormal dielectric behaviors in Mn-doped $CaCu_3Ti_4O_{12}$ ceramics and their response mechanism. Mater Sci Eng, B 177:1773–1776
23. Cai J, Lin YH, Cheng B, Nan CW, He J, Wu Y, Chen X (2007) Dielectric and nonlinear electrical behaviors observed in Mn-doped Ca $Cu_3Ti_4O_{12}$ ceramic. Appl Phys Lett 91:252905
24. Wang C, Ni W, Zhang D, Sun X, Wang J, Li H, Zhang N (2016) Dielectric properties of pure and Mn-doped $CaCu_3Ti_4O_{12}$ ceramics over a wide temperature range. J Electroceram 36:46–57
25. Mandal KD, Rai AK, Kumar D, Parkash O (2009) Dielectric properties of the $Ca_{1-x}La_xCu_3Ti_{4-x}Co_xO_{12}$ system ($x = 0.10$, 0.20 and 0.30) synthesized by semi-wet route. J Alloys Compd 10(478):771–776
26. Kim HE, Choi SM, Hong YW (2014) Improved dielectric properties of the $CaCu_3Ti_4O_{12}$ composites using $BaTiO_3$-coated powder as precursor. J Alloys Compd 610:594–599
27. Gautam P, Khare A, Sharma S, Singh NB, Mandal KD (2016) Characterization of $Bi_{2/3}Cu_3Ti_4O_{12}$ ceramics synthesized by semi-wet route. Prog Nat Sci Mater 26:567–571
28. Jia R, Zhao X, Li J, Tang X (2014) Colossal breakdown electric field and dielectric response of Al-doped $CaCu_3Ti_4O_{12}$ ceramics. Mater Sci Eng, B 185:79–85
29. Sun DL, Wu AY, Yin ST (2008) Structure, properties, and impedance spectroscopy of $CaCu_3Ti_4O_{12}$ ceramics prepared by sol–gel process. J Am Ceram Soc 91:169–173
30. Wu X, Huang K, Yuan L, Feng S (2018) Fabrication of ultralong perovskite structure nanotubes. RSC Adv 8:367–373
31. Huang CJ, Li K, Wu SY, Zhu XL, Chen XM (2015) Variation of ferroelectric hysteresis loop with temperature in $(Sr_xBa_{1-x})Nb_2O_6$ unfilled tungsten bronze ceramics. J Mater 1:146–152
32. Yadava SS, Singh L, Sharma S, Mandal KD, Singh NB (2016) Effect of temperature on the dielectric and ferroelectric properties of a nanocrystalline hexagonal $Ba_4YMn_3O_{11.5-\delta}$ ceramic synthesized by a chemical route. RSC Adv 6:68247–68253